PNAS
www.pnas.org

Supplementary Information for

Mechanosensitive channel gating by delipidation

Vanessa Judith Flegler, Akiko Rasmussen, Karina Borbil, Lea Boten, Hsuan-Ai Chen, Hanna Deinlein, Julia Halang, Kristin Hellmanzik, Jessica Löffler, Vanessa Schmidt, Cihan Makbul, Christian Kraft, Rainer Hedrich, Tim Rasmussen*, Bettina Böttcher*

*Corresponding authors: Tim Rasmussen and Bettina Böttcher
Email: Bettina.Boettcher@uni-wuerzburg.de; Tim.Rasmussen@uni-wuerzburg.de

This PDF file includes:

Supplementary Information Text

Materials & Methods

Materials. Chemicals were obtained from Sigma-Aldrich if not specified otherwise.

Expression and purification of MscS. Expression and purification of MscS has been described elsewhere (1–3) with only small modifications. The used construct with a pTrc vector as backbone expresses MscS with a C-terminal His6-tag. The *E. coli* strain MJF641 which has all genes for mechanosensitive channels deleted (4) was used for expression in Luria-Bertani medium induced with 0.8 mM IPTG for 4 hours at 30 ºC. Cells were harvested by centrifugation at 5000×g for 30 min and stored at -80 ºC until further use. Cells were suspended with 5 ml/g cells in a buffer containing 1 % (condition 2b and 3b) or 1.5 % (condition 1, 2a, 3a) dodecyl-β-maltoside (DDM; from Glycon, Germany), 50 mM sodium phosphate buffer pH 7.5, 300 mM NaCl, 10 % (w/v) glycerol, 5 mM EDTA, 10 mg/g cells lysozyme 50 mM imidazole and 1 mM phenylmethane sulfonyl fluoride and incubated on ice for 30 min. Then, 10 mM $MgCl_2$ and 0.01 % DNase (Roche) was added followed by further 30 min of incubation on ice. The suspension was centrifuged at 7000 g for 30 min and filtered through 0.2 µm syringe filters (Roth, Germany). MscS was bound to pre-packed 0.5 ml Ni-NTA agarose columns and washed with 30 ml of washing buffer containing either 0.05 % (condition 1), 0.5 % DDM (condition 2a-3a) or 0.03 % LMNG (condition 2b-3b), 50 mM sodium phosphate buffer pH 7.5, 300 mM NaCl, 10 % (w/v) glycerol, and 50 mM imidazole. For the elution, 300 mM imidazole in washing buffer was used. The peak fraction was further purified by size exclusion chromatography. For the DDM-solubilized samples (condition 1, 2a, 3a), the samples were injected on a Superdex200 Increase 10/300 column (GE Healthcare) equilibrated with buffer A containing 50 mM HEPES pH 7.5, 150 mM NaCl and 0.03 % DDM. For the LMNG samples, buffer A contained 0.02 % LMNG instead of DDM (condition 2b, 3b). Peak fractions for all detergent solubilized samples were concentrated in 100-kDa spin filters (Amicon) to 5 mg/ml and used for grid preparation. For condition 3a, the sample in condition 2a was supplemented with 0.1 mg/ml azolectin added from a stock solution of 10 mg/ml solved in 0.5% DDM and incubated for 30 min at room temperature before grid preparation. For condition 3b, 0.14 mg/ml BrPE was added (stock 14 mg/ml in 0.5 % LMNG) to a sample of MscS that was obtained under condition 2b. BrPE was used in an attempt to use bromine as marker for lipids in cryo-EM and for correlation to fluorescence studies. BrPE was synthesized from 1,2-dioleoyl-sn-glycero-3-phosphoethanolamine (DOPE) by bromination (5, 6). It should be noted that neither azolectin nor BrPE are native to *E. coli*. However, many studies used azolectin with little effect on the function of MscS (7, 8) while the molecular properties of brominated lipids are similar to their unsaturated counterparts (9).

Cryo-electron microscopy. All MscS samples were frozen on R1.2/1.3 holey carbon coated copper 400 grids (Quantifoil) employing a Vitrobot IV (FEI) freezing device with following settings: 7 sec blotting time, 25 blot force, 0 sec waiting time, 0 sec drain time, and 1 blot in total with a humidity of 100 % and temperature of 4 °C. Data were acquired at the cryoEM facility in Würzburg on a FEI Titan Krios G3 microscope equipped with a direct Falcon III detector (10). The magnification was set to 75,000 which corresponds to a calibrated pixel size of 1.0635 Å. The condenser aperture was set to 70 µm and the object aperture to 100 µm. Defocus values in the range from 1.0 to 2.2 µm were chosen (Table S2). Movies of 47 frames with a total dose of 80 e-/Å^2 and total time of 75 sec were recorded in counting mode. For the sample under condition 3b, movies of 40 frames with a total dose of 80 e-/Å^2 and total time of 5 sec were recorded in linear mode.

Single particle image processing and model building. Movies motion correction and dose weighting was performed with the program *MotionCor2* (11). For further data processing the workflow in *Relion* 3.1 was used (12). The contrast transfer functions were determined with the program *CTFFind4* (13). Particles were first auto-picked with the program *crYOLO* (14) and after

2D classification with appropriate class averages as references in *Relion* (15). Two rounds of 2D classification were performed to clean up particles, also rejecting projections along the C7 symmetry axis. An initial reference was obtained *ab initio* in Relion. CTFrefine in *Relion* was used for per-particle CTF correction and beam tilt correction. The resolution is given according to gold standard at a cut-off 0.143 as implemented in *Relion* (16) and for the local resolution the corresponding tool of *Relion* was used. The structures of MscS in azolectin nanodiscs (pdb: 6RLD) (17) or in DDM (pdb: 5AJI) (5) were used as starting models for molecular modelling in *Coot* version 0.9.2 (18). *Phenix* realspace.refine version 1.19-4092 (19) was used for the refinement of the model followed by validation with *MolProbity* (20). Images were generated with *Chimera* 1.14 (21) or *ChimeraX* (22). The data acquisitions and analyses are summarized in *SI Appendix*, Table S2.

Thin layer chromatography. MscS samples (500 µg), purified under conditions 1 and 2a, were extracted in a test tube in a mixture of chloroform, methanol and sample in a volume ratio of 1:2:0.8 (23). After vigorous mixing for 5 min, one part chloroform was added and mixed for 1 min followed by one part 1 M KCl and 1 min mixing. The tubes were centrifuged at 310 g for 5 min and the lower organic phase was transferred to a new test tube. The extract was dried in an argon stream and resolved in 25 µl chloroform for application on the TLC plate. A 20x20 cm^2 silica F254 aluminium plate was dried at 70°C for 10 min before application of the MscS extracts and lipid standards. A closed tank was lined with filter paper, filled and equilibrated with chloroform, methanol and 1 M KCl in a 10:10:3 volume ratio as mobile phase (5). The plate was placed in the tank und left until the mobile phase ascended two thirds of the plate. After drying of the plate, it was stained with 0.05 % (w/v) primuline in acetone:water (volume ratio 8:2) and spots were imaged under UV light (24). Then the plate was sprayed with 0.1 % ninhydrin (Thermo Fisher Scientific, Kandel, Germany) in acetone:water (volume ratio 8:2) followed by heating at 120°C until pink spots developed to specifically detect phosphoethanolamine (25).

Electrophysiological Experiments. Patch clamp experiments were carried out as previously described (6). In short, the inside out configuration of membrane patches was derived from E. coli giant protoplasts using E. coli strain MJF429 (*ΔyggB, ΔmscK*) transformed with pTrcMscS plasmid. The expression was induced for 10 minutes with 1 mM IPTG. The patch buffer used in the experiments contained 200 mM KCl, 90 mM $MgCl_2$, 10mM $CaCl_2$ and 5 mM HEPES with pH adjusted to 7.0. All data were acquired using a HEKA EPC8 amplifier and Patch Master software (Heka, Germany). Measurements were conducted on at least 6 patches derived from a minimum of two independent sample preparations. Pressure ratios P_L:P_S for activation of MscL in relation to MscS are given as mean ± standard deviation. This serves as measure for the tension required to open MscS independent of the patch diameter. The dwell time was analyzed with the software *Origin* 2019b with a bin size of 5 ms and fitting of a Gaussian distribution to the logarithmic dwell times.

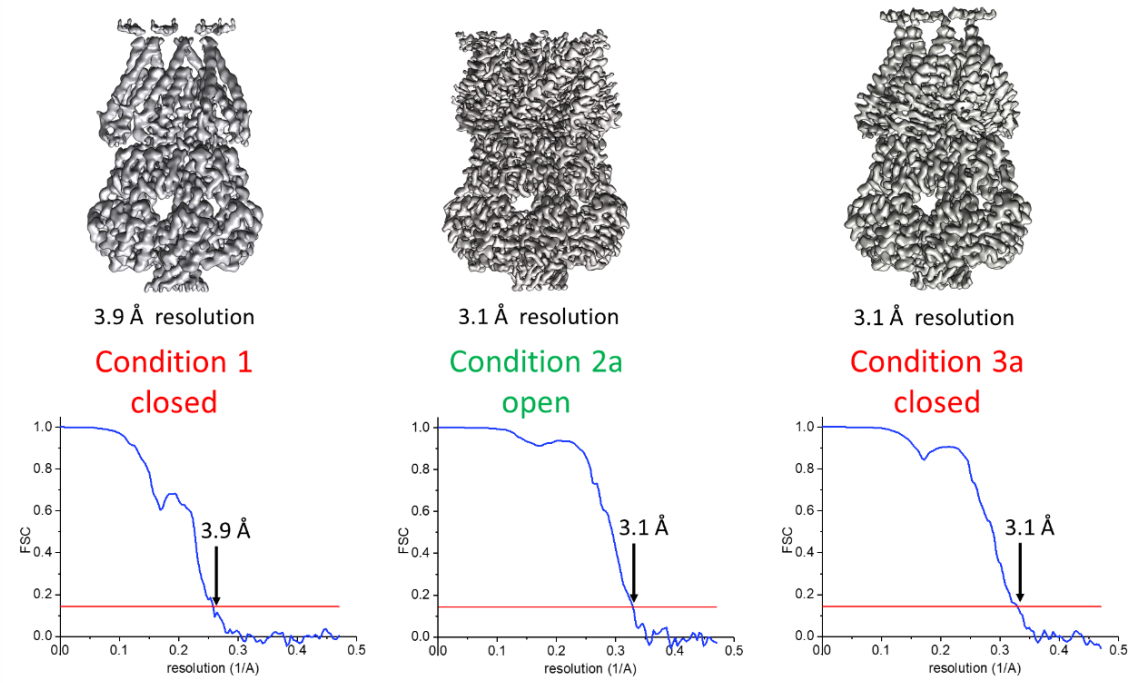

Figure S1. DDM-solubilized MscS in open and closed conformations.

MscS was solubilized in 1.5 % DDM for 1 h at 4°C and then purified in a 2-step protocol, with a Ni-NTA IMAC and SEC. MscS was incubated in wash buffer containing 0.05 % (condition 1) or 0.5 % DDM (condition 2a) overnight which switched MscS from the closed to the open conformation. Addition of DDM-solubilized azolectin (condition 3a) returned MscS to the closed conformation, confirming that the amount of associated lipid controls the conformational state of solubilized MscS. The Fourier Shell correlation (FSC) plot for the final refinement (top) are shown.

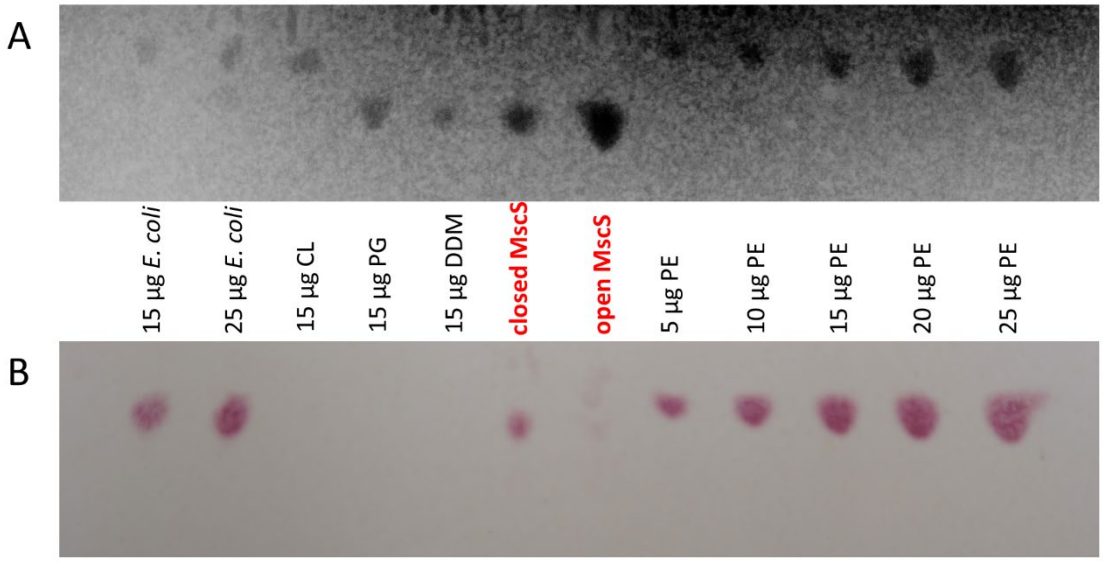

Figure S2. Thin layer chromatography of extracts from DDM-solubilized MscS.

Extracts of closed MscS (lane 6; condition 1) and open MscS (lane 7; condition 2a) were compared with different standards: E. coli polar lipid extract (lane 1 and 2), cardiolipin (lane 3; CL), phosphatidylglycerol (lane 4; PG), DDM (lane 5), and a concentration series of phosphatidylethanolamine (lane 8-12; PE). All lipids and DDM were visualized with primulin and UV lighting (A) and selectively PE with ninhydrin (B). In summary, for closed MscS a higher amount of PE and a lower amount of DDM is detected in comparison to open MscS.

Figure S3. Comparison of open MscS in DDM and LMNG.

The models of open MscS in DDM (grey, condition 2a) and LMNG (red, condition 2b) are overlaid showing a high degree of similarity.

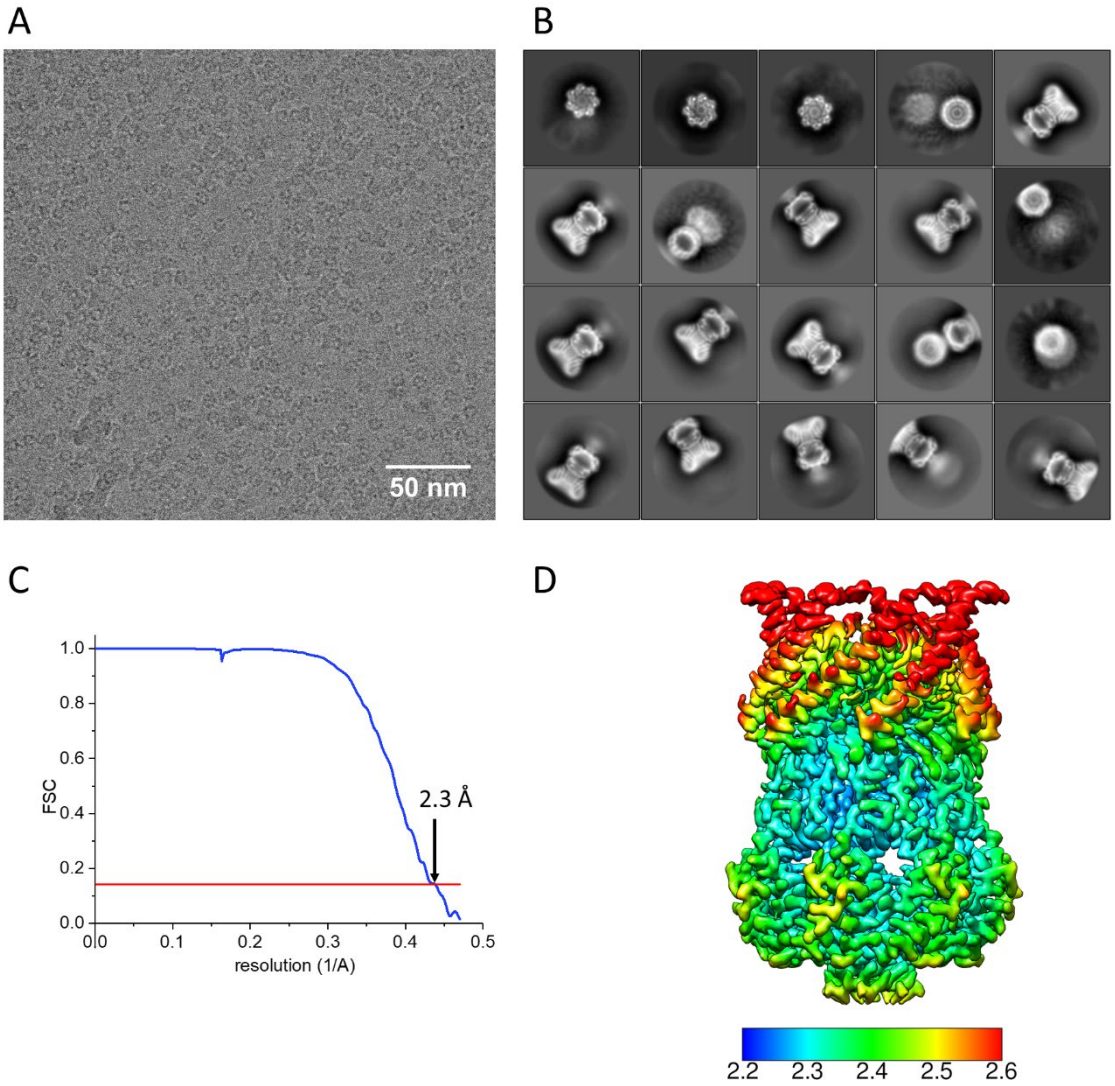

Figure S4. Cryo-EM of MscS in LMNG (condition 2b).

(A) Part of a typical micrograph. (B) An early 2D classification shows an approximately equal distribution between top and side views. The edge of each box corresponds to 27.2 nm. (C) The Fourier Shell Correlation (FSC) is shown for the final refinement. (D) The local resolution determined with the Relion local resolution tool.

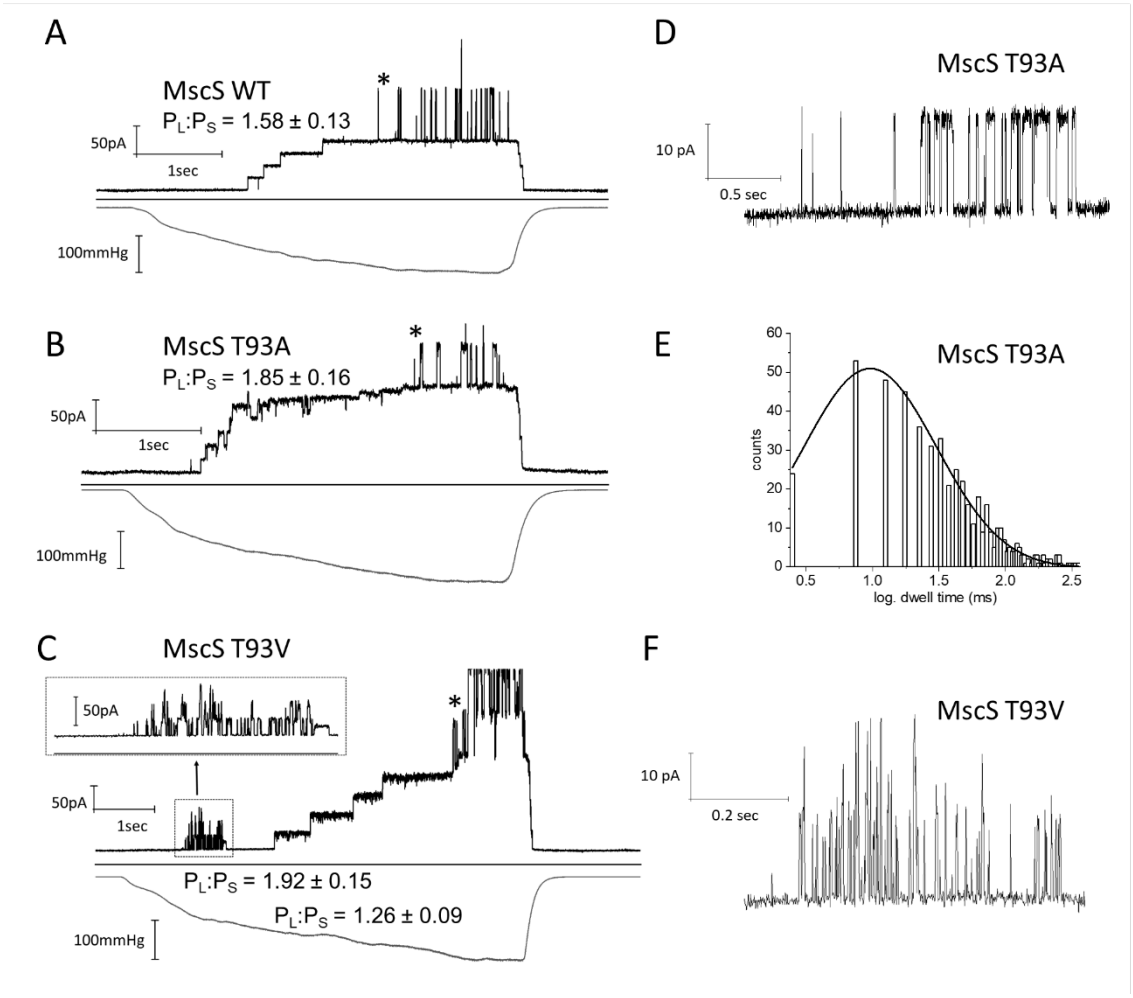

Figure S5. Electrophysiological characterization of T93 mutants.

Typical electrophysiological traces are shown for MscS WT (A), T93A (B) and T93V (C) together with the pressure traces (below, respectively). The pressure ratio to open MscL relative to MscS (PL:PS) is a measure for the required tension to open MscS. Openings of MscL are marked by *. T93A is easier to open than WT. T93V shows easier opening with a short dwell time and opening with normal dwell time at higher tensions than WT. (D) Dwell times were analyzed quantitively for T93A on recordings which had only single channel openings as shown here. (E) The log. dwell times were fitted to a Gaussian distribution which resulted a τ = 10 ± 15 msec. (F) This trace shows that the openings of MscS T93V at low pressures are not resolved and the dwell time is thus probably below 1 msec.

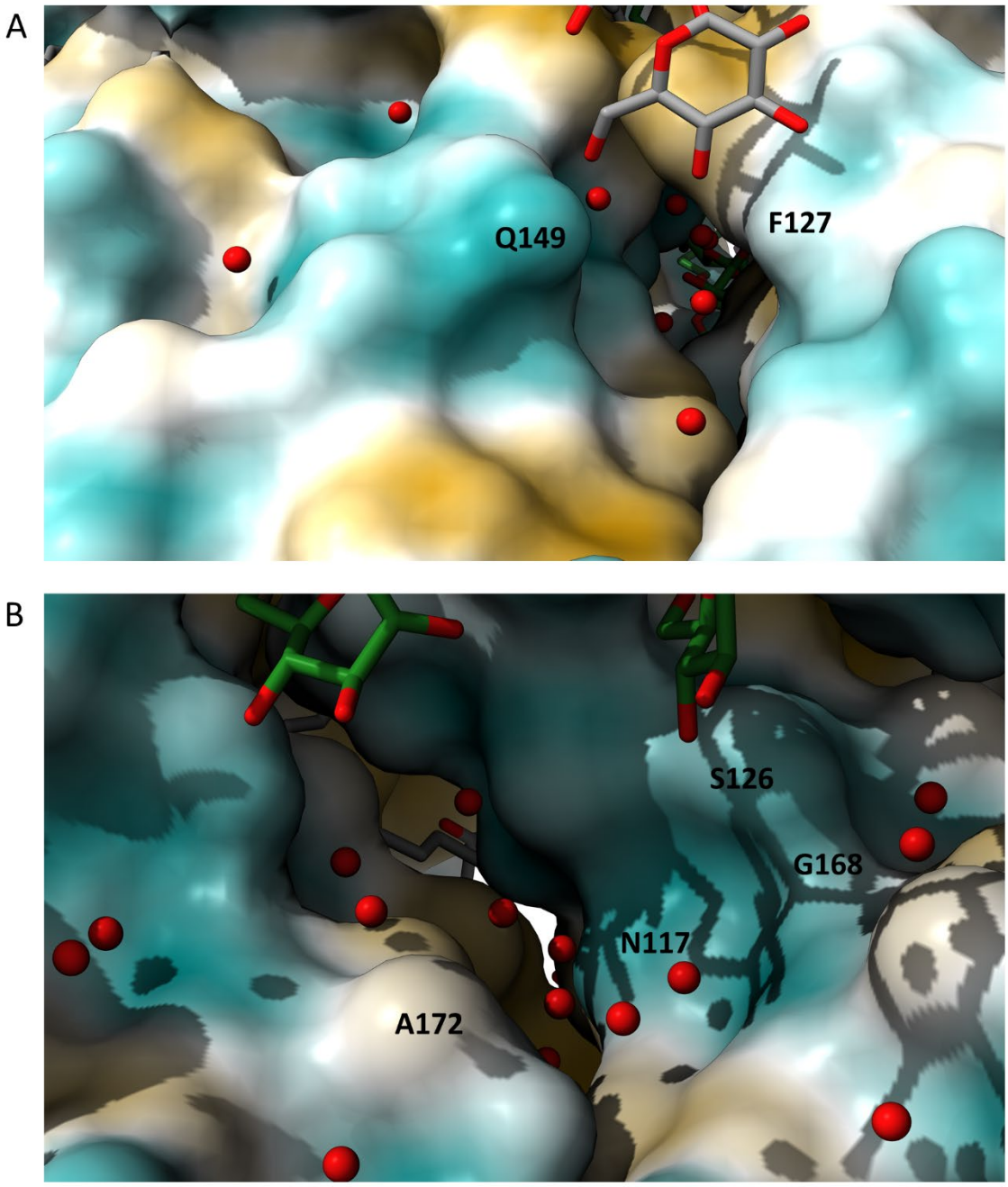

Figure S6. Water channel in the vestibule.

(A) View from outside of the vestibule into the water channel. (B) view from the inside. The hydrophobicity from hydrophilic (blue) to hydrophobic (brown) is shown on the surface-representation of the model. Water molecules are shown as red spheres, DDM molecules as green sticks, and LMNG molecules as grey sticks.

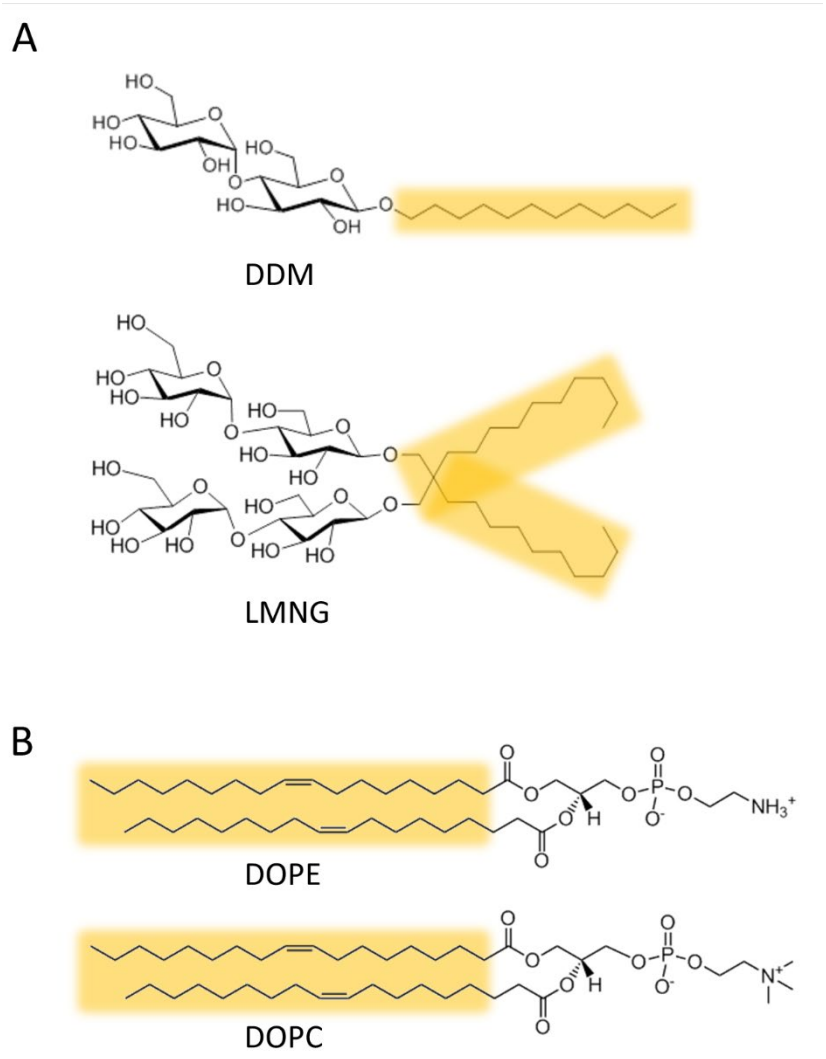

Figure S7. Chemical structures of ligands.

(A) used detergents and (B) lipids in this study. The hydrophobic regions are indicated in yellow.

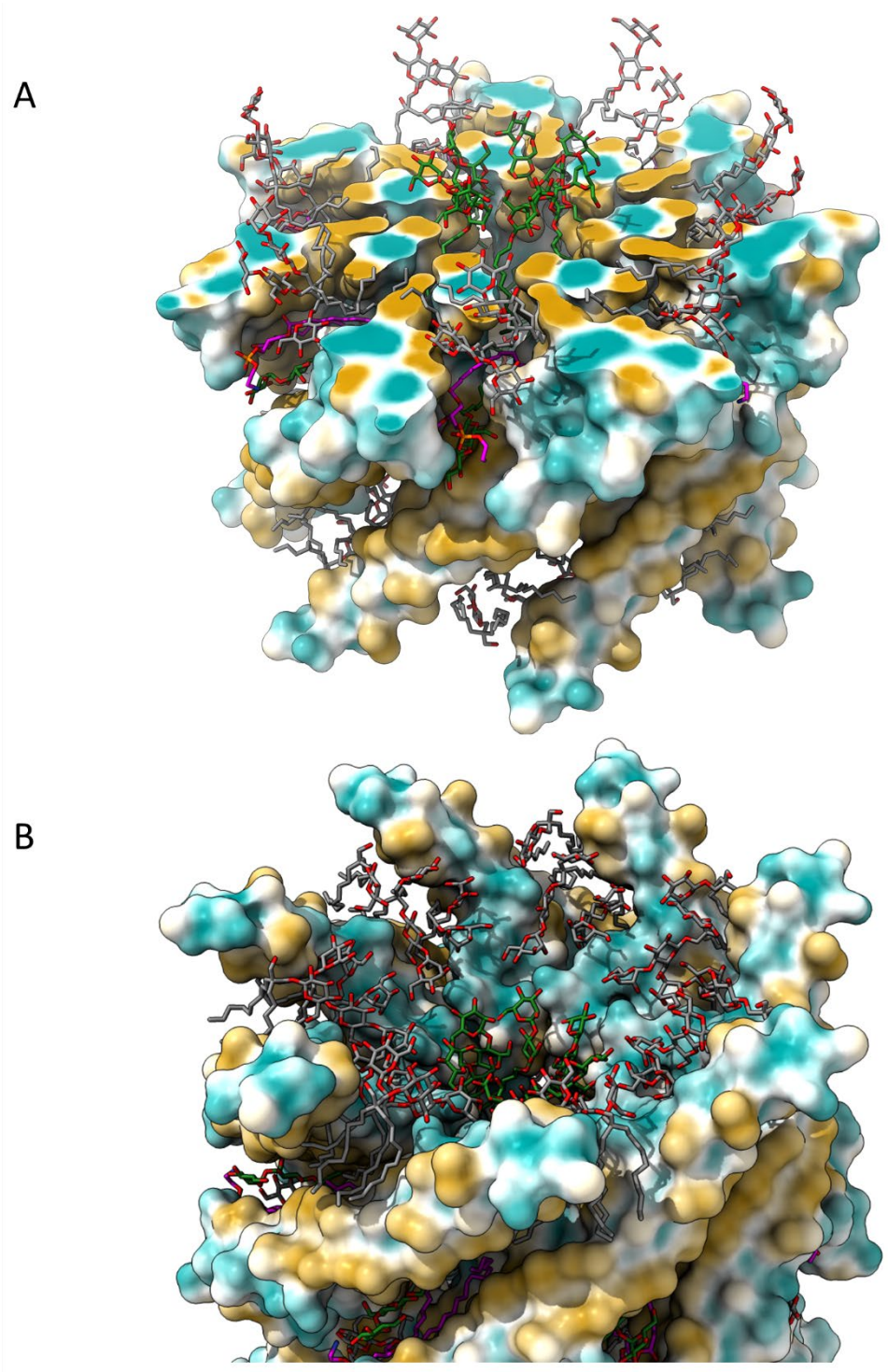

Figure S8. Ligand interaction with MscS solubilized in LMNG (condition 2b).

(A) Cut through MscS at the height of the paddle loops. View from the cytosolic side. (B) view from the periplasmic side into the funnel. LMNG molecules between TM1 helices face with their hydrophilic head groups towards the funnel. The hydrophobicity is shown from hydrophilic (blue) to hydrophobic (brown) on the surface-representation of the MscS model. The lipid is shown as magenta sticks, DDM molecules as green sticks, and LMNG molecules as grey sticks.

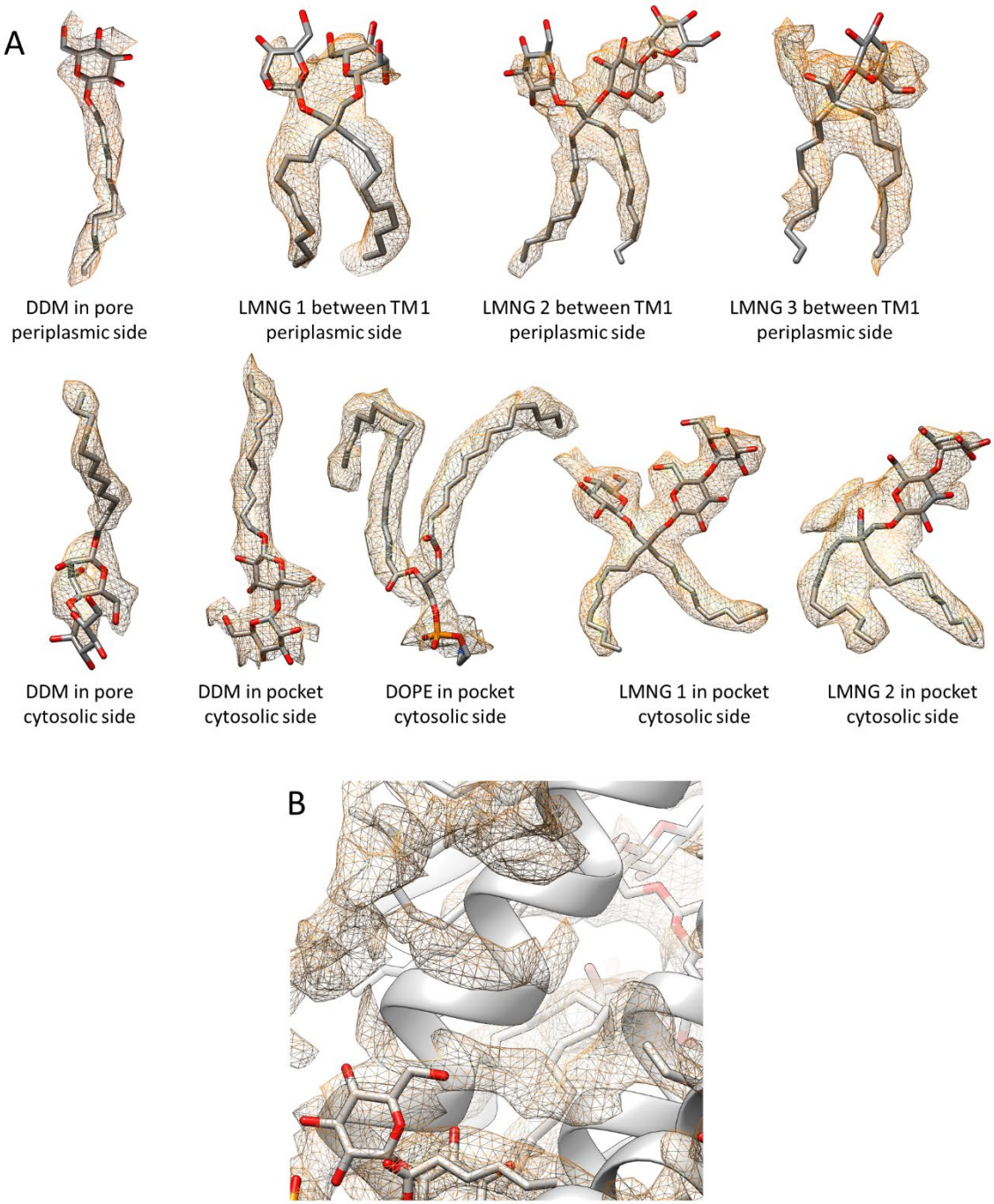

Figure S9. Ligand interaction with MscS solubilized in LMNG (condition 2b).

(A) 9 ligands are resolved per subunit in the structure of MscS in LMNG (condition 2b). Models are shown together with their densities. In the top row the ligands on the periplasmic side are shown, on the bottom row the ligands on the cytosolic side. (B) Some density is not modelled in the grooves between the paddles on the cytosolic side, beside densities from the N-terminal domain and micelle. A difference map without protein densities is shown at a level of 1.5 σ.

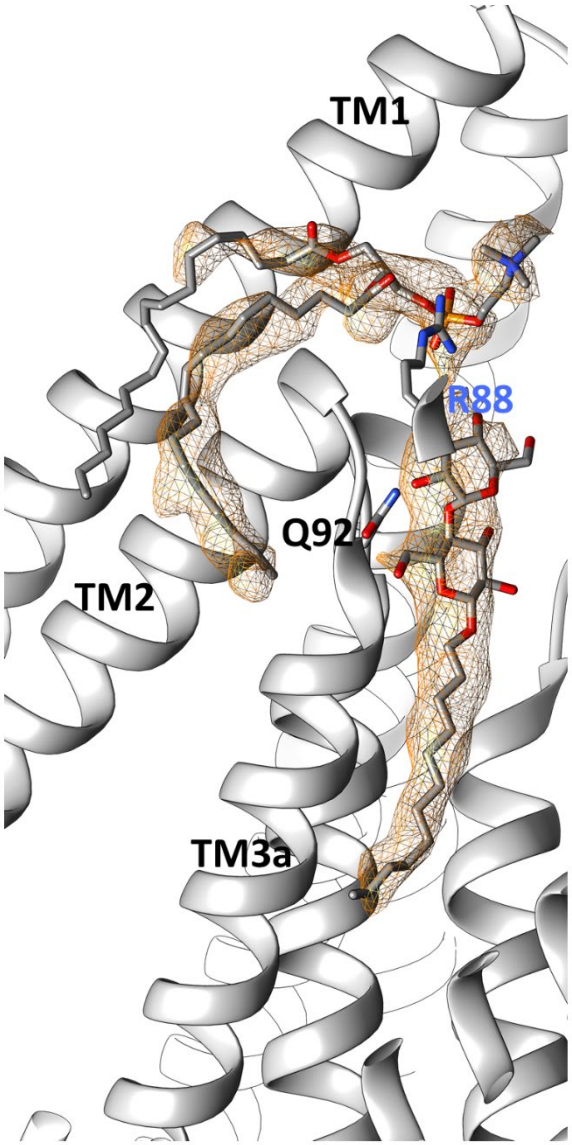

Figure S10. Ligands in the structure of MscS solubilized in DDM with added lipids (condition 3a).

At the loop between TM2 and TM3a, the periplasmic entrance to the pore, a lipid is resolved similar to a lipid seen in the nanodisc structures. One fatty acid chain of this lipid is not well resolved. R88 forms a salt bridge with the phosphate group (this R88 residue from the neighboring subunit to the front is the only residue shown from this subunit for clarity). Q92 from the neighboring subunit on the other side (back) is binding the DDM head group. These two ligands are also seen in the closed DDM-solubilized sample under condition 1.

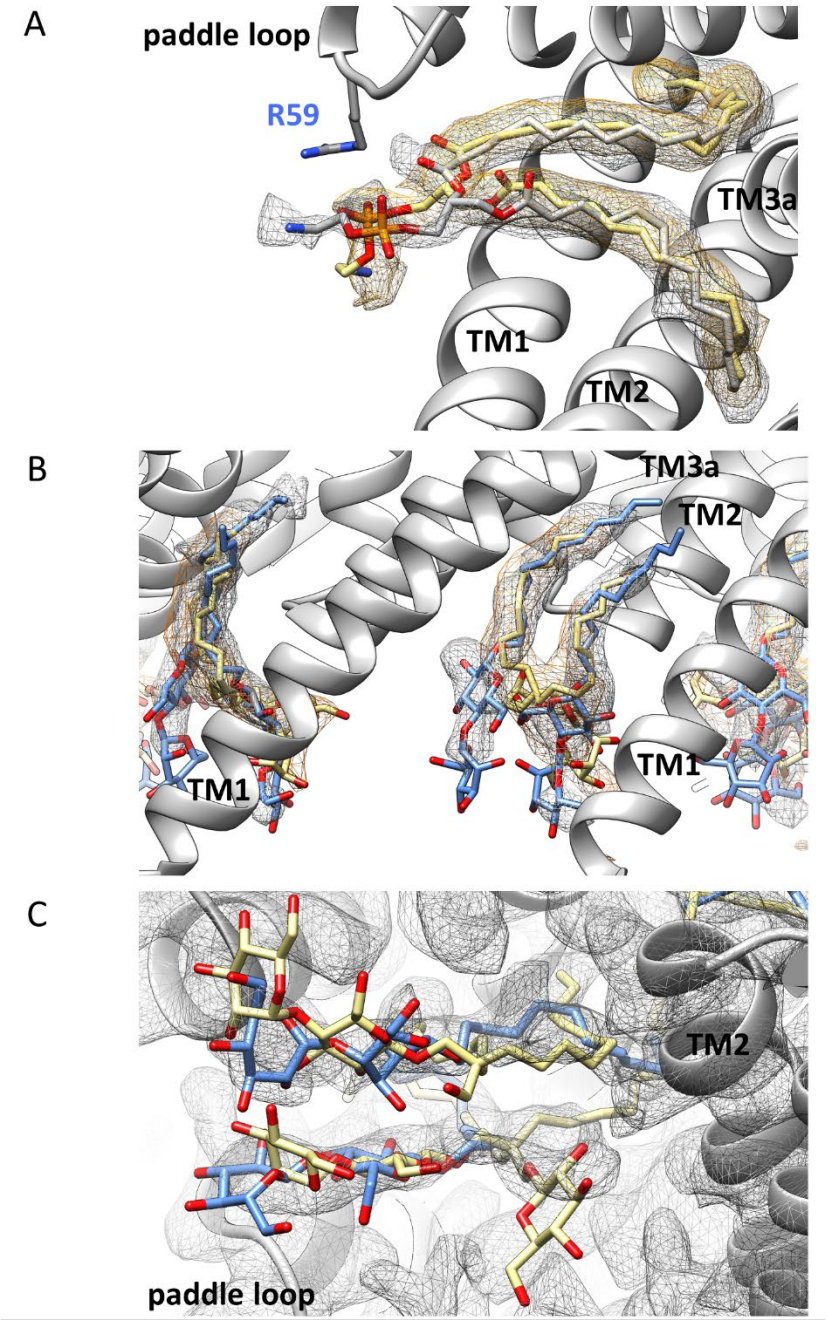

Figure S11. Comparison of ligands in the open structures.

(A) The lipid at the paddle loop takes the same bent conformation for the fatty acid chains in the DDM structure (condition 2a; grey) in comparison to the LMNG structure (condition 2b; yellow) while the head groups are slightly different. (B) On the periplasmic side, tails of two DDM molecules can be identified (blue) at the loop between TM2 and TM3a corresponding to the best resolved LMNG molecule (yellow) on the periplasmic side in the LMNG structure (see Fig. 5 A). (C) In the open DDM structure two layers of densities are seen between the paddle loop and TM3b (grey) which were modelled as two DDM molecules (blue). The tails are not well resolved, and additional densities are unexplained. These two layers seen in the map correspond to two stacked LMNG molecules (yellow) seen in the LMNG structure (see Fig. 5 B).

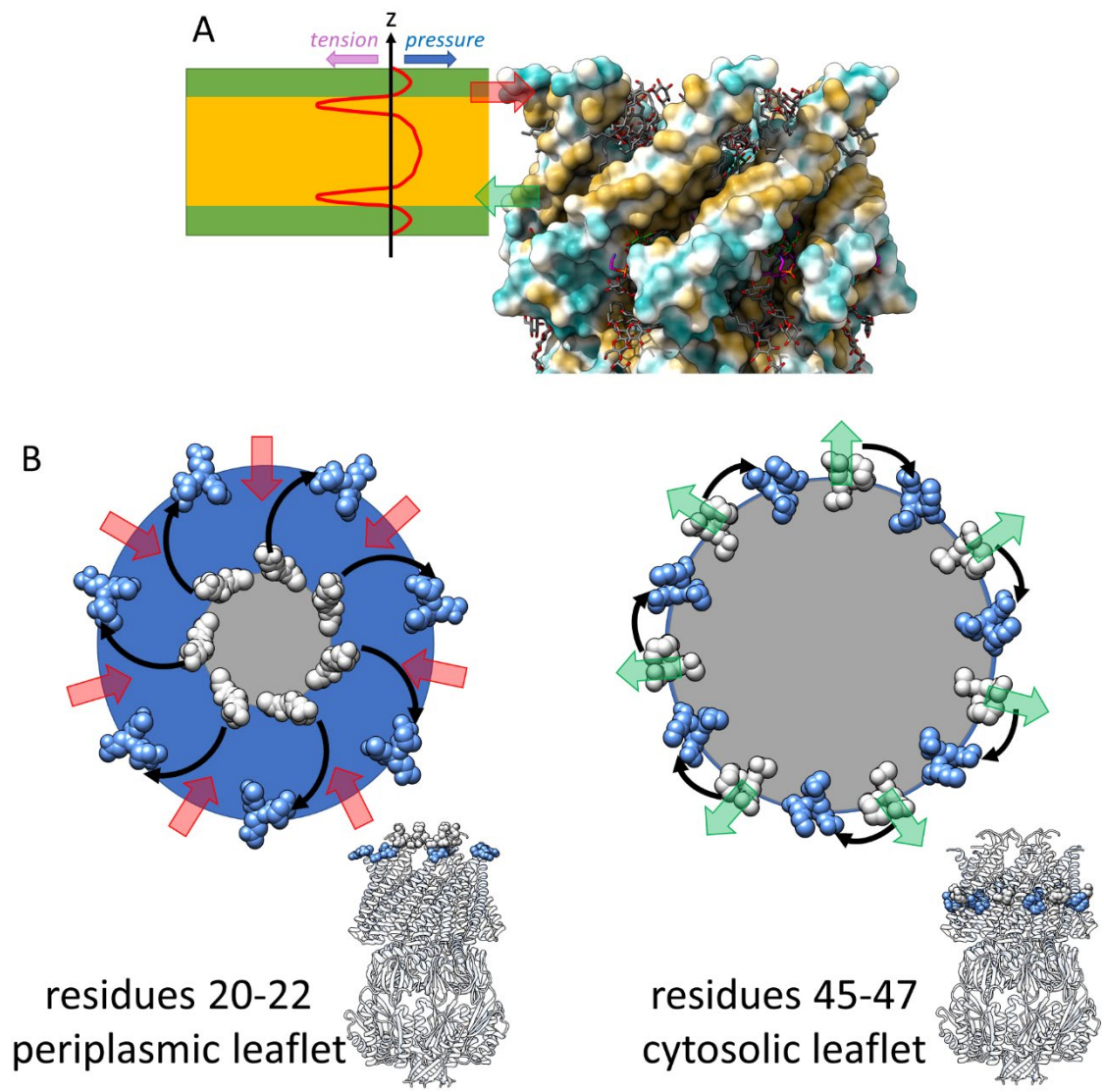

Figure S12. Gating transition in the regions of highest membrane tension.

(A) The pressure profile over the membrane is highly anisotropic with tension at the onset of the acyl chains and positive pressure in the head groups and the membrane core (red line). The region of highest tension must be most important for tension sensing and the approximate contact on open MscS is shown on the right. (B) This region corresponds on the periplasmic leaflet to the N-terminus of TM1 at residues 20-22 (left side) and on the cytosolic leaflet approximately to resides 45-47 (right side). These residues are shown as spheres for the closed (grey) and open (blue) conformation. The covered area (colored circles, viewed from the periplasmic side) changes dramatically on the periplasmic side but not at all on the cytosolic side but gaps appear between the TM1 helices on the periplasmic side during gating where lipids can move in with their head groups facing the water bulk phase within the funnel (red arrows). On the cytosolic leaflet, the grooves release lipids (green arrows) because the total volume of the cytosolic hydrophobic pockets decreases due to the outward moving pore helices.

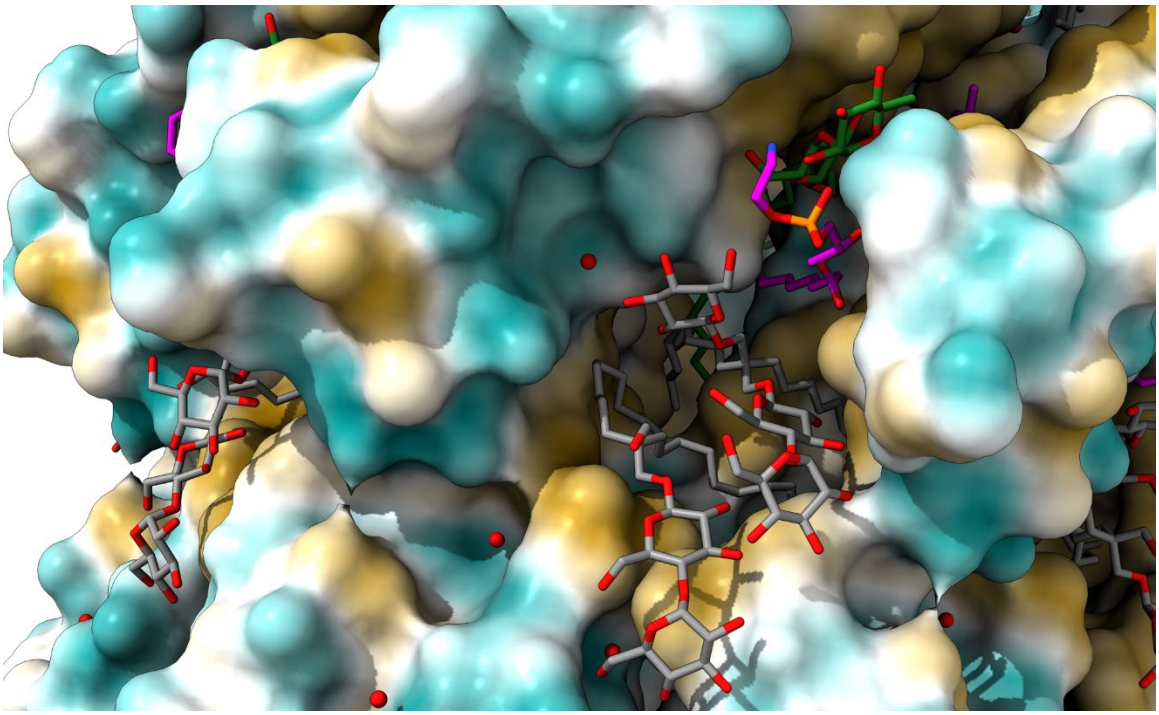

Figure S13. Hydrophobic patch between paddle and cytosolic domain in the structure of MscS solubilized in LMNG (condition 2b).

A hydrophobic pocket opens up to the cytosolic water bulk phase between the paddles (top) and the cytosolic domain (bottom). This large opening is covered by two LMNG molecules (grey) in the LMNG solubilized sample. In the groove between the paddles also a lipid molecule (magenta) and a DDM molecule (green) are resolved. The hydrophobicity is shown from hydrophilic (blue) to hydrophobic (brown) on the surface-representation of the MscS model.

Table S1. Structural alignment with reference structures.

Structures obtained in this study which had a different degree of delipidation were compared with reference structures from the literature. For this the models were aligned in Chimera with the matchmaker tool and then the RMSD values (Å) where determined for the best fitting subunits until residue G113. That is the region where predominantly differences are seen between the different states. The closest match is marked in red. All structures in this study correspond to the open and closed conformations but not to the recently described sub-conducting or desensitized states (26). Note that the desensitized state described by Zhang et al. (26) corresponds to the inactivated state described by Akitake et al. (27) as judged by the behavior of the mutant G113A (marked as *). Reference structures 6VYK, 6VYL, 6VYM were from Zhang et al. (26) and 2VV5 from Wang et al. (28).

reference structures (PDB)			**6VYK**	**2VV5**	**6VYL**	**6VYM**
assigned state			*closed*	*open*	*sub-conducting*	*desensitized (inact.*)*
condition 1	7ONL	low DDM	**2.2**	**14.9**	**12.5**	**13.8**
condition 2a	7OO0	high DDM	**15.5**	**0.7**	**4.3**	**23.8**
condition 3a	7OO6	high DDM + lipid	**2.3**	**14.5**	**12.3**	**14.2**
condition 2b	7ONJ	LMNG	**15.4**	**0.7**	**4.4**	**23.7**
condition 3b 1st conformation	7OO8	LMNG + lipid	**2.2**	**14.8**	**12.5**	**14.1**
condition 3b 2nd conformation	7OOA	LMNG + lipid	**15.3**	**0.7**	**4.4**	**23.7**

Table S2. EM data collection and modelling.

	DDM solubilized MscS			LMNG solubilized MscS		
	condition 1 closed	**condition 2a open**	**condition 3a closed**	**condition 2b open**	**condition 3b open**	**condition 3b closed**
EMDB code	**EMD-12997**	**EMD-13003**	**EMD-13006**	**EMD-12996**	**EMD-13008**	**EMD-13007**
Data collection						
Microscope	Titan Krios G3				Titan Krios G3	
Voltage (kV)	300				300	
Camera	Falcon III EC				Falcon III EC	
Data collection mode	counting				linear	
Electron dose ($e^-/Å^2$)	80				80	
Underfocus (μm)	1.2 – 2.2	1.2 – 2.2	1.2 – 2.2	1.0 – 2.0	1.0 – 1.8	
Pixel size (Å)	1.0635	1.0635	1.0635	1.0635	1.0635	
Number of movies collected	1,859	6,287	2,262	3,292	10,080	
Map parameters						
Final number of particles	140,826	841,492	399,384	232,197	262,797	43,500
Symmetry imposed	C7	C7	C7	C7	C7	C7
Map resolution (Å)	3.9	3.1	3.1	2.3	2.7	3.7
Sharpening *B*-factor ($Å^2$)	-235	-138	-174	-50	-75	-113
Modelling						
PDB code	7ONL	7OO0	7OO6	7ONJ	7OOA	7OO8
Model composition						
Non-hydrogen atoms	13923	16016	14546	17717	15610	13923
Protein residues	1827	1834	1827	1834	1834	1827
Ligands	0	56	14	63	35	0
Validation						
MolProbity Score	1.31	1.58	1.48	1.47	1.31	1.31
Clashscore	5.72	7.27	9.05	8.68	5.68	5.72
Poor rotamers (%)	0.20	0.00	0.00	0.47	0.00	0.47
R. m. s. deviations						
Bond lengths (Å)	0.002	0.007	0.003	0.008	0.003	0.003
Bond angles (°)	0.379	0.624	0.413	0.667	0.440	0.393
Ramachandran plot						
Favored (%)	98.46	96.92	98.46	99.23	99.62	98.07
Allowed (%)	1.54	3.08	1.54	0.77	0.38	1.93
Outliers (%)	0.00	0.00	0.00	0.00	0.00	0.00

SI References

1. T. Rasmussen, *et al.*, Properties of the Mechanosensitive Channel MscS Pore Revealed by Tryptophan Scanning Mutagenesis. *Biochemistry* **54**, 4519–30 (2015).
2. T. Rasmussen, *et al.*, Tryptophan in the pore of the mechanosensitive channel MscS: assessment of pore conformations by fluorescence spectroscopy. *J. Biol. Chem.* **285**, 5377–84 (2010).
3. A. Rasmussen, *et al.*, The role of tryptophan residues in the function and stability of the mechanosensitive channel MscS from Escherichia coli. *Biochemistry* **46**, 10899–908 (2007).
4. M. D. Edwards, *et al.*, Characterization of three novel mechanosensitive channel activities in Escherichia coli. *Channels* **6**, 272–81 (2012).
5. C. Pliotas, *et al.*, The role of lipids in mechanosensation. *Nat. Struct. Mol. Biol.* **22**, 991–998 (2015).
6. T. Rasmussen, *et al.*, Interaction of the Mechanosensitive Channel, MscS, with the Membrane Bilayer through Lipid Intercalation into Grooves and Pockets. *J. Mol. Biol.* **431**, 3339–3352 (2019).
7. F. Xue, *et al.*, Membrane stiffness is one of the key determinants of E. coli MscS channel mechanosensitivity. *Biochim. Biophys. Acta - Biomembr.* **1862**, 183203 (2020).
8. T. Nomura, *et al.*, Differential effects of lipids and lyso-lipids on the mechanosensitivity of the mechanosensitive channels MscL and MscS. *Proc. Natl. Acad. Sci. U. S. A.* **109**, 8770–5 (2012).
9. J. East, A. Lee, Lipid selectivity of the calcium and magnesium ion dependent adenosine triphosphatase, studied with fluorescence quenching by a brominated phospholipid. *Biochemistry* **21**, 4144–4151 (1982).
10. B. Song, *et al.*, Capabilities of the Falcon III detector for single-particle structure determination. *Ultramicroscopy* **203**, 145–154 (2019).
11. S. Q. Zheng, *et al.*, MotionCor2: Anisotropic correction of beam-induced motion for improved cryo-electron microscopy. *Nat. Methods* **14**, 331–332 (2017).
12. S. H. W. Scheres, RELION: Implementation of a Bayesian approach to cryo-EM structure determination. *J. Struct. Biol.* **180**, 519–530 (2012).
13. A. Rohou, N. Grigorieff, CTFFIND4: Fast and accurate defocus estimation from electron micrographs. *J. Struct. Biol.* **192**, 216–221 (2015).
14. T. Wagner, *et al.*, SPHIRE-crYOLO is a fast and accurate fully automated particle picker for cryo-EM. *Commun. Biol.* **2**, 218 (2019).
15. S. H. W. Scheres, Semi-automated selection of cryo-EM particles in RELION-1.3. *J. Struct. Biol.* **189**, 114–122 (2015).
16. S. H. W. Scheres, S. Chen, Prevention of overfitting in cryo-EM structure determination. *Nat. Methods* **9**, 853–854 (2012).
17. T. Rasmussen, V. J. Flegler, A. Rasmussen, B. Böttcher, Structure of the Mechanosensitive Channel MscS Embedded in the Membrane Bilayer. *J. Mol. Biol.* **431**, 3081–3090 (2019).
18. P. Emsley, B. Lohkamp, W. G. Scott, K. Cowtan, Features and development of Coot. *Acta Crystallogr. Sect. D Biol. Crystallogr.* **66**, 486–501 (2010).
19. P. D. Adams, *et al.*, PHENIX: A comprehensive Python-based system for macromolecular structure solution. *Acta Crystallogr. Sect. D Biol. Crystallogr.* **66**, 213–221 (2010).
20. V. B. Chen, *et al.*, MolProbity : all-atom structure validation for macromolecular crystallography. *Acta Crystallogr. Sect. D Biol. Crystallogr.* **66**, 12–21 (2010).
21. E. F. Pettersen, *et al.*, UCSF Chimera - A visualization system for exploratory research and analysis. *J. Comput. Chem.* **25**, 1605–1612 (2004).
22. E. F. Pettersen, *et al.*, UCSF ChimeraX : Structure visualization for researchers, educators, and developers. *Protein Sci.* **30**, 70–82 (2021).
23. E. G. Bligh, W. J. Dyer, A rapid method of total lipid extraction and purification. *Can. J. Biochem. Physiol.* **37**, 911–917 (1959).
24. V. P. Skipski, Thin-Layer Chromatography of Neutral Glycosphingolipids. *Methods*

Enzymol. **35**, 396–425 (1975).
25. V. P. Skipski, R. F. Peterson, M. Barclay, Quantitative analysis of phospholipids by thin-layer chromatography. *Biochem. J.* **90**, 374–378 (1964).
26. Y. Zhang, *et al.*, Visualization of the mechanosensitive ion channel MscS under membrane tension. *Nature* **590**, 509–514 (2021).
27. B. Akitake, A. Anishkin, N. Liu, S. Sukharev, Straightening and sequential buckling of the pore-lining helices define the gating cycle of MscS. *Nat. Struct. Mol. Biol.* **14**, 1141–9 (2007).
28. W. Wang, *et al.*, The structure of an open form of an E. coli mechanosensitive channel at 3.45 A resolution. *Science* **321**, 1179–1183 (2008).